


Thermal assisted up-conversion electroluminescence in quantum dot light emitting diodes

Qiang Su¹ & Shuming Chen ^{1,2}✉

Up-conversion electroluminescence, in which the energy of a emitted photon is higher than that of the excitation electron, is observed in quantum-dot light-emitting diodes. Here, we study its mechanism by investigating the effect of thermal energy on the charge injection dynamic. Based on the results of temperature-dependent electroluminescence and theoretical analysis, we reveal that at sub-bandgap voltage, holes can be successfully injected into quantum-dots via thermal-assisted thermionic-emission mechanism, thereby enabling the sub-bandgap turn-on and up-conversion electroluminescence of the devices. Further theoretical deduction and experimental results confirm that thermal-assisted hole-injection is the universal mechanism responsible for the up-conversion electroluminescence. This work uncovers the charge injection process and unlocks the sub-bandgap turn-on mechanism, which paves the road for the development of up-conversion devices with power conversion efficiency over 100%.

¹Department of Electrical and Electronic Engineering, Southern University of Science and Technology, Shenzhen 518055, People's Republic of China. ²Key Laboratory of Energy Conversion and Storage Technologies (Southern University of Science and Technology), Ministry of Education, Shenzhen 518055, People's Republic of China. ✉email: chen.sm@sustech.edu.cn

The past decade has witnessed the fast development of quantum-dot (QD) light-emitting diodes (QLEDs), which are considered to be the ideal candidates for next generation displays because they are self-emitting and have the advantages of high color saturation, high efficiency and low cost processibility^{1–8}. Typical QLEDs consist of a p-type polymeric hole transport layer (HTL), a QD emitter and a n-type ZnO electron transport layer (ETL), which are sequentially stacked and sandwiched between a transparent anode and a metallic cathode^{1–10}. By applying a voltage, electrons and holes can overcome the potential barrier and inject into the QDs, subsequently forming the electron-hole pairs (excitons) that are bound by their Coulombic attraction. The radiative recombination of excitons leads to the generation of photons with energy of $h\nu$, which is roughly equal to or slightly smaller than the bandgap energy (E_g) of the QDs. Because the photons are converted from the electrons, the energy of the injected electrons at a applied voltage of V should thus be equal to the energy of photons, i.e., $eV = h\nu \approx E_g$, which implies that the minimum applied voltage or the turn-on voltage V_T to induce detectable electroluminescence (EL) should satisfy $V_T \geq h\nu/e$. However, it has been frequently observed that the V_T is substantially smaller than $h\nu/e$ ^{1,3–5,11} for instance, we found that the turn-on voltage to induce a 620 nm red emission in typical QLEDs can be as low as 1.2 V (Supplementary movie), which is far smaller than the bandgap voltage of 2 V and means that an electron with energy of 1.2 eV can be up-converted to a 2.0 eV photon. The phenomena of sub-bandgap turn-on and up-conversion EL have also been observed in III-V compound semiconductor LED^{12–14}, Rubrene/Fullerene organic LED^{15–17} and MEH-PPV/ZnO LED¹⁸, but the mechanism remains unclear and is still under debate.

For typical QLEDs driven by a sub-bandgap voltage, electron injection into QDs is relatively efficient, but hole injection into QDs is extremely difficult because of the presence of the hetero-junction barrier, and thus most holes have to accumulate at the hetero-interface of QDs/HTL¹⁹. Therefore, unveiling the hole injection process is the key to unlock the mechanism of up-conversion EL. Most reports conclude that hole injection into QDs is enabled by an Auger-assisted process^{1,2,4,20}, in which the interfacial excitons formed between the injected electrons and the accumulated holes resonantly transfer their energy to the proximal holes, thereby providing extra energy to the holes and assisting them to overcome the barrier and inject into the QDs. In such a process, the formation of one QD exciton should consume an interfacial exciton, and thus the maximum internal quantum efficiency (IQE) is limited to 50% and thus the maximum external quantum efficiency (EQE) is lower than 10% by assuming a typical outcoupling efficiency of 20–25%⁶. However, most efficient QLEDs can exhibit a high EQE of over 10% even driven by a sub-bandgap voltage^{3,5,21}, thereby disapproving the Auger-assisted mechanism. Another negative evidence is the turn-on voltage to induce a detectable EL is smaller than that required to create the interfacial excitons²². Therefore, the Auger process is unlikely responsible for the up-conversion EL. Recently, Chen et al. revealed that the turn-on voltage of red QLEDs is approximately equal to the flat-band (FB) voltage of the QD layer and they concluded that when the QD layer reaches the FB state, holes are able to inject into the QDs via the field-assisted thermionic-emission mechanism²², which seems reasonable to explain the up-conversion EL. Very recently, Jin et al. deciphered the exciton-generation processes in QLEDs and suggested that hole injection is assisted by confinement-enhanced Coulomb interactions²³, which enables the devices to exhibit efficient EL at sub-bandgap voltage.

Considering that the mechanism for the up-conversion EL is still under debate, it is of fundamental interest to find out the true origin.

Here, we address a fundamental question of how the holes are injected into the QDs at sub-bandgap bias. By investigating the temperature-dependent EL including current–voltage–luminance (J–V–L), capacitance–voltage (C–V) and transient EL characteristics, we are able to probe the effect of thermal energy on the charge injection dynamic. We reveal that thermal energy play an essential role in the sub-bandgap charge injection processes. At sub-bandgap bias, holes can be successfully injected into QDs via thermal-assisted thermionic-emission mechanism, thereby enabling the sub-bandgap turn-on and up-conversion EL of the devices. Our findings uncover the charge injection process and unlock the sub-bandgap turn-on mechanism, which could encourage the development of up-conversion QLEDs with power conversion efficiency over 100%.

Results

Thermal-assisted up-conversion EL. The effect of thermal energy on the EL characteristics of the QLEDs (with a regular structure of glass/ITO/PEDOT: PSS/TFB/QD/ZnMgO/Al) was investigated by varying the temperature during measurement. Fig 1a–c show the temperature-dependent luminance–voltage characteristics of the red, the green and the blue QLEDs, respectively. See Supplementary Figs. 1 and 2 for relevant performance and detailed discussion. At room temperature (RT), all devices exhibit sub-bandgap turn-on characteristics; for instance, the turn-on voltages (V_T) to induce a luminance of 0.1 cd m^{-2} of red (620 nm), green (532 nm) and blue (470 nm) emission are 1.6, 1.8 and 2.3 V, respectively, which are remarkably lower than their corresponding photon voltages ($V_{ph} = h\nu/e$) of 2.0, 2.3 and 2.6 V, consequently resulting in the up-conversion efficiencies (V_{ph}/V_T) or gains of 125%, 128% and 113%, respectively. Interestingly, the V_T is significantly affected by the temperature; for example, for the red QLEDs, the V_T is decreased to 1.25 V at an elevated temperature of 160 °C, while it is increased and approached to the bandgap voltage of 2.03 V by cooling down the devices to –100 °C. It should be noted that, even at a sub-bandgap applied voltage, the EL spectra are identical to those at high voltage (Supplementary Fig. 3), indicating that the emission is originated from the QDs. At a sub-bandgap bias of 1.6 V, the up-conversion EL is switched on at RT and is gradually enhanced when the temperature is further elevated, as demonstrated in Fig. 1g and Supplementary Movie 1. Similar phenomena are also observed in green and blue QLEDs. As shown in Fig. 1d, the EL spectra are also modulated by the temperature, which are red-shifted when the temperature is increased. This is because temperature can induce the expansion of the crystal lattice, thereby leading to the shrinkage of the QD bandgap, as well-explained by the Varshni relation²⁴. To investigate whether the variation of V_T is caused by the change of the photon energy, we compare the V_T and V_{ph} at different temperatures. As shown in Fig. 1e, for the red QLEDs, when the temperature is increased, the V_T is significantly reduced (from 2.12 to 1.25 V), while the V_{ph} is mildly decreased (from 2.04 to 1.95 V), and as a result, the up-conversion efficiency is rapidly increased from 96% to 156%. These results indicate that: (1) the reduction of V_T at elevated temperatures should not be attributed to the change of V_{ph} , but instead, should be ascribed to the increase of the thermal energy; (2) the sub-bandgap turn-on and up-conversion EL are enabled by the thermal-assisted charge injection process. It is likely that thermal energy can effectively promote the charge injection, as will be discussed later. With higher thermal energy provided, more charges can be injected into QDs, thereby leading to the reduction of V_T and the improvement of up-conversion efficiency, as reflected in Fig. 1e. It should be noted that the Auger-assisted charge injection process is excluded, because the devices exhibit an EQE of 12.5%

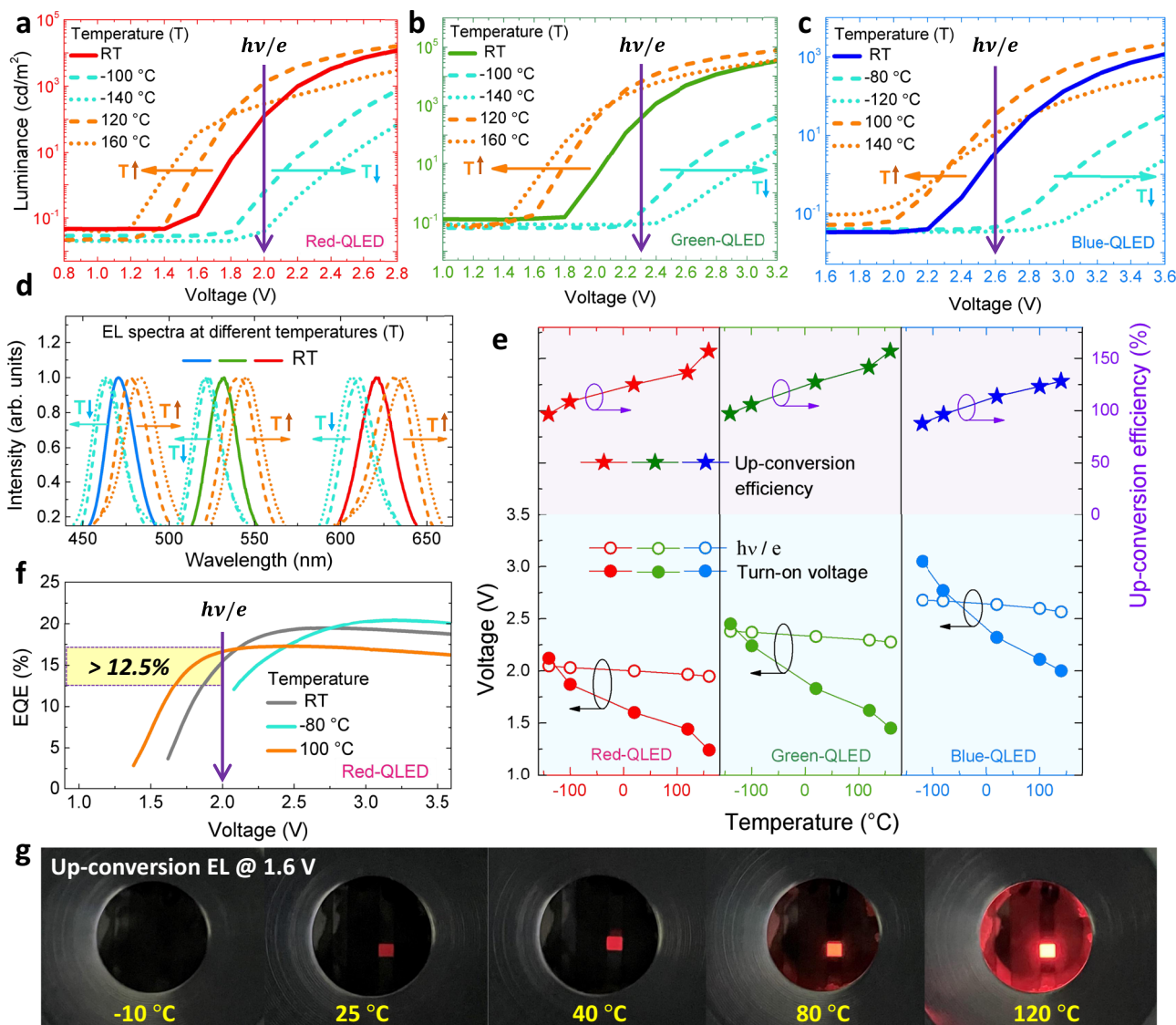


Fig. 1 Temperature-dependent EL characteristics. The luminance-voltage (L-V) characteristics of **a** red-, **b** green-, and **c** blue-QLEDs under different temperatures (RT= room temperature): the V_T (turn-on voltage) is remarkably reduced as the temperature is increased. **d** EL spectra of red-, green- and blue-QLEDs at different temperatures (the orange/blue arrows represent an increase/decrease in temperature). **e** The V_T (solid circle), photon voltage V_{ph} ($V_{ph} = h\nu/e$, open circle) and up-conversion efficiency (star) of red-, green- and blue-QLEDs at different temperatures: the up-conversion efficiency is gradually increased as the temperature is increased, indicating that the up-conversion EL is triggered by a thermal-assisted process. **f** EQE-V characteristics of red-QLEDs at different temperatures: at sub-bandgap bias of 1.7-2.0 V, the devices exhibit an EQE of 12.5-15%, which is higher than the upper limit (~10%) of the Auger-assisted process, thus disapproving the Auger-assisted mechanism. **g** Photographs of up-conversion EL at 1.6 V under different temperatures: the luminance is gradually increased as the temperature is elevated (also demonstrated in Supplementary Movie 1).

~15% at a sub-bandgap bias of 1.7–2.0 V (Fig. 1f), which is higher than the upper limit of ~10% of the Auger process. At elevated temperatures, although the charge injection is promoted (Supplementary Fig. 1) and the brightness is enhanced, the EQE is reduced (Fig. 1f) due to the damage of QDs and the quenching of excitons. As shown in Supplementary Fig. 2, at elevated temperatures, the electrons are delocalized to the surface traps first and then relax back to the core and recombine with the confined holes²⁴, thereby leading to the prolonged exciton lifetime (Supplementary Fig. 2b). In such a thermal-assisted recombination process²⁴, the quenching possibility is increased and thus the photoluminescence (PL) intensity of QDs is reduced (Supplementary Fig. 2a).

Charge-injection processes in QLEDs. To understand how the charges are injected into QDs at sub-bandgap bias, the charge injection processes are analyzed. Fig 2a shows the energy levels of each functional layer of the red QLEDs. For simplicity, we assume ohmic contacts are achieved so that hole injection from anode into TFB and electron injection from cathode into ZnMgO are very efficient. The electrons can be readily injected from ZnMgO into QDs due to the negligible barrier of QDs/ZnMgO heterojunction, while hole injection from TFB into QDs is extremely difficult as a high heterojunction barrier (ΔE_V) of:

$$\Delta E_V = E_{V_QD} - E_{HOMO_TFB} \quad (1)$$

is presented at the TFB/QDs interface, where E_{V_QD} and

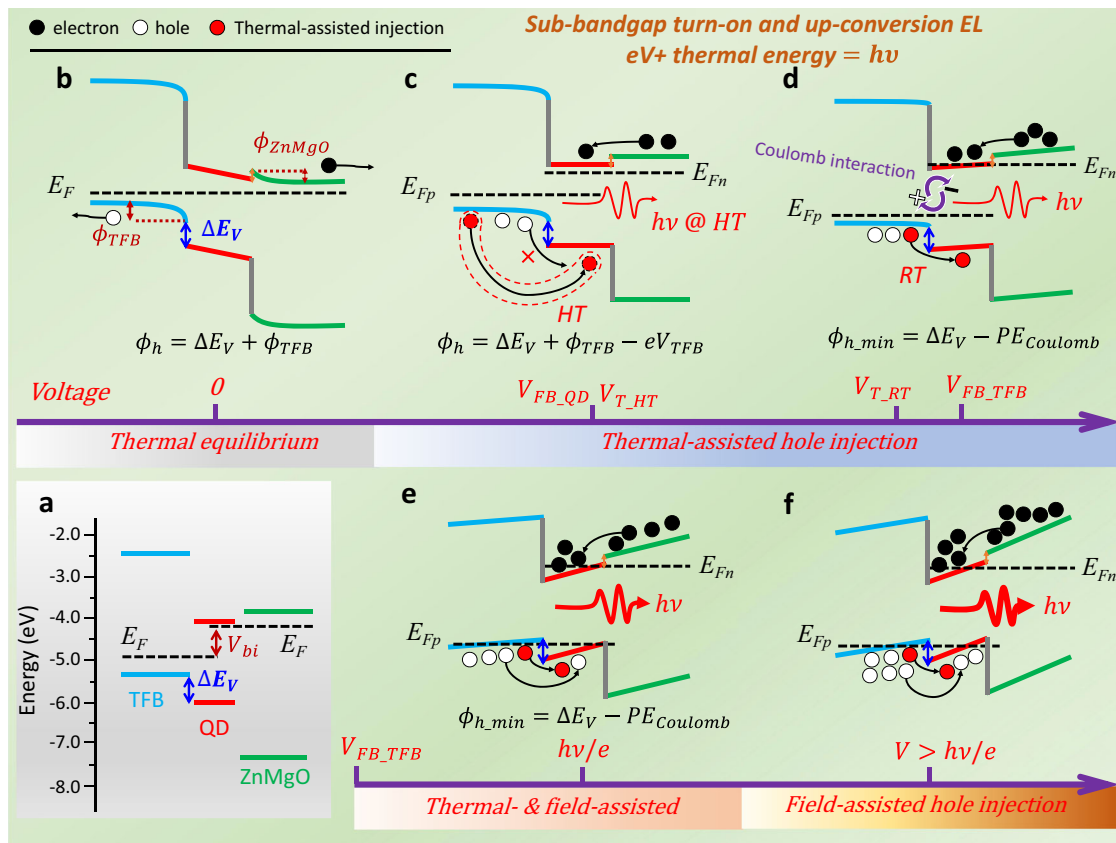


Fig. 2 Charge injection processes in QLEDs. **a** Energy levels of the functional layers of the typical red-QLEDs. **b** At thermal equilibrium, the surfaces of TFB and ZnMgO are depleted so that the Fermi levels are aligned through the system. Due to the presence of built-in surface potentials (ϕ_{TFB} and ϕ_{ZnMgO}), charge injection is impossible. **c** At V_{FB_QD} , flat-band is achieved in QD layer and thus electron injection into QDs is possible, while hole injection is still unfavorable due to the large injection barrier ϕ_h . However, at high temperature (HT), with sufficient thermal energy provided, holes could be injected into QDs via the thermal-assisted thermionic-emission mechanism. **d** At V_{FB_TFB} , flat-band is achieved in TFB layer, and the hole injection barrier is reduced to a minimum value of $\phi_h = \Delta E_V - PE_{Coulomb}$. At RT, with the assistance of thermal energy, the holes can overcome a barrier of 0.4 eV and injected into QDs. **e** At $h\nu/e$, all depletion regions are vanished and the electric field in all layers turn positive, and thus the holes can be accelerated towards the QDs. Hole injection is enabled by both thermal- and field-assisted thermionic-emission mechanisms. **f** At $V > h\nu/e$, due to the presence of strong positive electric field in TFB, hole injection is mainly dominated by the field-assisted thermionic-emission mechanism.

E_{HOMO_TFB} are the valance band levels of QDs and TFB, respectively. Under different applied voltages, the charge injection process is analyzed as below:

(1) $V = 0V$. At thermal equilibrium, the surfaces of TFB and ZnMgO are depleted so that the Fermi levels are aligned through the system, as displayed in Fig. 2b. Because of the existence of surface depletion layer, built-in surface potentials ϕ_{TFB} and ϕ_{ZnMgO} are created at the surface of TFB and ZnMgO, respectively. In this situation, injection of holes and electrons is impossible because they will be pulled back by the negative built-in potentials.

(2) $0 < V \leq V_{FB_QD}$ (V_{FB_QD} defined as the flat-band voltage of QDs). The applied voltage, which is in opposite direction to the built-in potentials, is mainly dropped across the depletion layers. As shown in Fig. 2c, when the applied voltage is increased to V_{FB_QD} , corresponding to the flat-band voltage of QDs, electron injection into QDs becomes possible, while hole injection from the depleted TFB into QDs is still unfavorable due to the presence of injection barrier. The hole injection barrier is determined by:

$$\phi_h = \Delta E_V + \phi_{TFB} - eV_{TFB} \quad (2)$$

where V_{TFB} is the effective applied voltage that is dropped across the depletion region of TFB. The accumulated electrons in QDs tend to attract the holes in TFB via the Coulombic

interaction^{23,25}. The potential energy of holes induced by the Coulombic interaction ($PE_{Coulomb}$) is:

$$PE_{Coulomb} = \frac{e^2}{4\pi\epsilon_0\epsilon_r x} \quad (3)$$

where x is the distance between electrons and holes, and ϵ_0 , ϵ_r are the vacuum dielectric permittivity and the relative dielectric constant of TFB, respectively. Considering the Coulombic interaction, the injection barrier then is modified as (also shown in Supplementary Figure 4):

$$\phi_h = \Delta E_V + \phi_{TFB} - eV_{TFB} - PE_{Coulomb} \quad (4)$$

It should be noted that when the surface of TFB is depleted, the $PE_{Coulomb}$ could be neglected because electrons and holes are separated by a long distance. If the kinetic energy of holes (E_K), gained from thermal energy, is larger than ϕ_h , then the holes can be injected into QDs via the thermionic-emission mechanism^{14,25}. At RT and V_{FB_QD} , it is difficult to observe the EL; however, at high temperature (HT), with sufficient thermal energy provided, thermal-assisted hole injection could be triggered, thereby enabling the turn-on of EL at V_{FB_QD} . It should be noted that the V_{FB_QD} is the minimum voltage to initiate the EL²², and thus by measuring the lowest V_T , the V_{FB_QD} can be accessed. As

shown in Supplementary Fig. 5, when the temperature is increased from 160 to 240 °C, the V_{T-HT} (turn-on voltage at HT) cannot be further reduced and is fixed at ~1.2 V, which represents the lowest V_T and therefore marks the value of V_{FB-QD} . A general picture to describe the up-conversion EL is that, at V_{FB-QD} , an electron with energy of 1.2 eV can be directly injected into QDs, while with the assistance of thermal energy, a hole can overcome the ϕ_h and inject into QDs, thereby producing a 2.0 eV photon with a up-conversion gain of 167%. Based on the energy conservation law, the hole injection barrier of 0.8 eV can readily be deduced by subtracting the electron electrostatic energy from the photon energy.

(3) $V_{FB-QD} < V \leq V_{FB-TFB}$ (Fig. 2d, V_{FB-TFB} defined as the flat-band voltage of TFB). As the V_{TFB} dropped across the depleted TFB is increased, the ϕ_h is gradually reduced. For example, when the applied voltage is increased to 1.6 V, we can detect the 2.0 eV photons at RT, indicating that the ϕ_h is reduced to 0.4 eV. When the applied voltage is further increased to V_{FB-TFB} , corresponding to the flat-band voltage of TFB, the build-in ϕ_{TFB} is completely canceled, and thus the ϕ_h is reduced to a minimum value of:

$$\phi_{h\text{-min}} = \Delta E_V - PE_{Coulomb} \quad (5)$$

At V_{FB-TFB} , holes accumulation at the TFB/QD interface becomes possible and thus the $PE_{Coulomb}$ cannot be neglected, which is estimated to be ~0.1 eV by substituting the radius of QDs ($x = 5$ nm) into Eq. (3). The V_{FB-TFB} , as determined by measuring the open-voltage V_{oc} (Supplementary Fig. 6) or the electro-absorption spectra of the devices²², is slightly higher than the RT turn-on voltage of 1.6 V, indicating that the $\phi_{h\text{-min}}$ is smaller than 0.4 eV, which is reasonable and is in consistent with reported values^{1,3-5,11,19,23}.

(4) $V_{FB-TFB} < V \leq hv/e$ (Fig. 2e). As the applied voltage is larger than V_{FB-TFB} , all depletion layers are vanished, and thus the applied voltage is mainly dropped across all layers. In this situation, the electric field in all layers turn positive, and thus the holes can be accelerated towards the QDs. The injection barrier is fixed at $\phi_{h\text{-min}}$. Now, the holes can gain their E_K from both electric field and thermal energy, and thus hole injection is co-governed by the thermal-assisted and the field-assisted thermionic-emission mechanisms.

(5) $V > hv/e$ (Fig. 2f). When the applied voltage is larger than the photon voltage, a strong positive electric field is present in all layers. Most holes can gain their E_K from the positive electric field and thus hole injection into QDs is mainly dominated by the field-assisted thermionic-emission mechanism. Very strong EL can be observed due to efficient charge injection.

From above analysis, we conclude that hole injection at sub-bandgap applied voltage, is mainly enabled by the thermal-assisted thermionic-emission mechanism, in which the holes can gain their E_K from the thermal energy, consequently allowing them to overcome a barrier up to 0.8 eV at a applied voltage of 1.2 V and leading to the generation of 2.0 eV up-conversion photons.

Thermal-assisted hole-injection. A question remains unresolved is whether the thermal energy kT is sufficiently high enough to assist the holes overcoming the ϕ_h . The kT at RT is only 0.026 eV, which seems too low to support the holes to overcome a barrier of 0.4 eV. However, it should be noted that the kT is a statistical average energy of many particles. Considering the thermal fluctuation, there has a probability that the energy of a specific particle is significantly higher than the average value, as described by the Boltzmann distribution law²⁶. For the holes, the probability of finding them at a certain energy E is defined by a more rigorous

Fermi-Dirac distribution law²⁵:

$$f_h(E) = \frac{1}{1 + \exp\left(\frac{E_F - E}{kT}\right)} \quad (6)$$

where E_F is the Fermi level of TFB. The probability of finding the holes as a function of E is plotted in Fig. 3a. It is obvious that even at RT, there has a certain probability [$f_h(E_{V-QD})$] for the holes to overcome the barrier ϕ_h , and inject into the valence band of QDs. When the temperature is elevated, the probability of hole injection into QDs is significantly increased. The amount of holes (per volume) that can be injected into QDs can be deduced by:

$$p = N_v e^{-\frac{E_F - E_{HOMO-TFB} + \phi_h}{kT}} = N_v e^{-\frac{E_F - E_{HOMO-TFB}}{kT}} e^{-\frac{\phi_h}{kT}} = p_0 e^{-\frac{\phi_h}{kT}} \quad (7)$$

where N_v is the effective density of state of TFB and p_0 is the hole concentration (number of holes cm^{-3}) in TFB. Equation (7) implies that hole injection into QDs is affected by both temperature and injection barrier, which is the typical characteristics of the thermionic-emission mechanism. From above discussion, at RT, the holes can gain the E_K from thermal energy and overcome a ϕ_h of 0.4 eV, that is:

$$E_K = \frac{1}{2} m_h v_h^2 = \phi_h \quad (8)$$

where m_h is the hole effective mass in TFB, and v_h is the velocity of the holes that can overcome the barrier. Per unit area and per second, the amount of holes (number of holes $\text{cm}^{-2}\text{s}^{-1}$) that can be injected into QDs is:

$$N = p \times v_h = p_0 e^{-\frac{\phi_h}{kT}} \times \sqrt{\frac{2\phi_h}{m_h}} \quad (9)$$

Assuming all injected holes are used to generate the photons, then the photon flux per unit area (number of photons $\text{cm}^{-2}\text{s}^{-1}$) is:

$$\varphi = N \quad (10)$$

The luminance (cd m^{-2}) can then be calculated by:

$$L = \frac{\varphi \times hv \times \eta \times \eta_{oc}}{\Omega} = \frac{p_0 \times hv \times \eta \times \eta_{oc}}{\Omega} \times e^{-\frac{\phi_h}{kT}} \times \sqrt{\frac{2\phi_h}{m_h}} \quad (11)$$

where η is the luminous efficacy (lm/W) of photopic vision, η_{oc} is the outcoupling efficiency of the device and Ω is the solid angle of the emission. By substituting $p_0 = 2.5 \times 10^{11} \text{ cm}^{-3}$ ²⁷, $hv = 2\text{eV}$, $\eta = 260 \text{ lm/W}$, $\eta_{oc} = 25\%$, $\Omega = 3.14$, $\phi_h = 0.4\text{eV}$, $m_h = 9.1 \times 10^{-31} \text{ kg}$ into Eq. (11), the luminance at a applied voltage of 1.6 V (corresponding to an injection barrier of 0.4 eV) can be calculated. As shown in Fig. 3b, the calculated luminance agrees fairly well with the measured value when the temperature is lower than 80 °C. At higher temperature, the measured value is higher than the calculated one, and this is because a constant p_0 is used to calculate the luminance, while at high temperature, the hole concentration of TFB can be significantly higher than p_0 due to thermal excitation, thus leading to the underestimation of the calculation. At low temperature, it is reasonable to use a constant p_0 because the population of thermally generated holes is too low to affect the p_0 . The above theoretical deduction and calculated results, which are based on classical carrier distribution and thermionic emission model, confirm that at RT, the holes can indeed overcome a barrier of 0.4 eV and inject into QDs via the thermal-assisted thermionic-emission mechanism, which consequently leads to the generation of detectable EL of 0.12 cd m^{-2} at a sub-bandgap voltage of 1.6 V.

The thermal-assisted hole injection can further be proved experimentally. Figure 3c shows the J-V of a hole-only-device

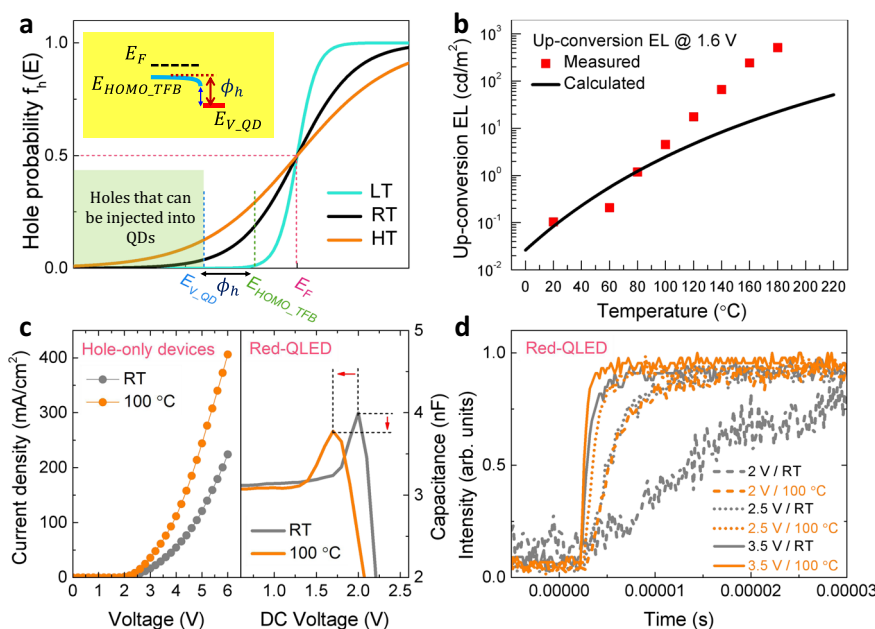


Fig. 3 Thermal-assisted hole-injection. **a** The probability of finding the holes at different energy: when the temperature is elevated, the probability that the holes can be injected into QDs is remarkably increased. **b** Up-conversion EL at 1.6 V under different temperatures: the calculated results agree fairly well with the measured one when the temperature is lower than 80 °C. At high temperature, the discrepancy is caused by the thermal excitation that increases the hole concentration of TFB. **c** The current density (J)- V characteristics of hole-only devices and capacitance- V characteristics of the red QLEDs at RT and 100 °C: at elevated temperature, the hole current is substantially enhanced, which thus reduces the peak capacitance of the devices. **d** The transient EL of red-QLEDs: at elevated temperature, the devices are turned-on more rapidly due to enhanced hole injection.

under different temperatures. At elevated temperature, the hole current is substantially enhanced, and as a result, the amount of the accumulated electrons is effectively reduced by recombining with the injected holes. Consequently, the peak capacitance of the devices is reduced and shifted to the low voltage region, as demonstrated in Fig. 3c. Moreover, at elevated temperature, the device turns-on more rapidly, as disclosed by the transient EL (Fig. 3d), which also suggests that hole injection is substantially enhanced by increasing the temperature. The thermal energy, not only assists the holes to overcome the barrier, but also promotes the hopping transport of the holes²⁸; both are contributed to an improved hole-injection.

Finally, we show that the thermal-assisted hole-injection is a universal mechanism for the up-conversion EL observed in different structured and different colored QLEDs. The up-conversion EL has been commonly observed in regular structured CdSe-based or InP-based (Supplementary Fig. 7) QLEDs with TFB HTL and ZnO-based ETL. By replacing the TFB with PVK or CBP, it is difficult to observe the up-conversion EL at RT, because the hole injection, which is significantly affected by p_0 and ϕ_h , in these devices are completely different to that in devices with TFB HTL. However, as shown in Fig. 4, when the temperature is varied, all devices exhibit the same temperature-dependent EL characteristics. Although these devices are built with different HTLs and different architectures, they all show the up-conversion EL at elevated temperature, which can be well explained by the universal thermal-assisted hole-injection mechanism.

Discussion

In summary, we address a fundamental question of how the holes are injected into the QDs at sub-bandgap bias that results in the up-conversion EL. Based on the experimental results of temperature-dependent EL, we reveal that thermal energy plays an essential role in the sub-bandgap charge injection processes. Theoretical analysis discloses the detail of the hole injection

processes under different applied bias. Our results show that at RT and at an applied voltage of 1.6 V, an electron with energy of 1.6 eV can be directly injected into QDs, while with the assistance of thermal energy, a hole can overcome a barrier of 0.4 eV and inject into QDs, thereby resulting in a 2 eV up-converted photon. The up-conversion gain can be higher than 167% by increasing the temperature. Further theoretical deduction and experimental results confirm that thermal-assisted hole-injection is the universal mechanism responsible for the up-conversion EL. Our findings uncover the charge injection process and unlock the up-conversion EL mechanism, which could encourage the development of up-conversion QLEDs with power conversion efficiency over 100%.

Methods

Materials. All materials are commercially available. CdSe-based colloidal red-/green-/blue-QDs were purchased from Suzhou Xingshuo Nanotech Co., Ltd. ZnMgO nanoparticles were purchased from Guangdong Poly Optoelectronics Co., Ltd. Poly[(9,9-dioctylfluorenyl-2,7-diyl)-co-(4,4'-(N-(p-butylphenyl)diphenylamine))] (TFB) were purchased from American Dye Source, Inc. Poly(3,4-ethylenedioxythiophene)-poly(styrenesulfonate) (PEDOT:PSS), Poly(9-vinylcarbazole) (PVK), and 4,4'-Bis(9-carbazolyl)-1,1'-biphenyl (CBP) were purchased from Luminescence Technology Corp. Molybdenum trioxide (MoO₃), chlorobenzene, and octane were purchased from Aladdin Industrial Corp. Absolute ethanol were purchased from ShangHai LingFeng Chemical Reagent Co., Ltd. ITO glass (20 Ω /sq) were purchased from Wuhu Jinghui Electronic Technology Co., Ltd.

Device fabrication. QLEDs with regular structures of glass/ITO/PEDOT:PSS (45 nm)/TFB (40 nm)/QDs (~15 nm)/ZnMgO (40 nm)/Al (100 nm) and glass/ITO/PEDOT:PSS (45 nm)/PVK (40 nm)/QDs (~15 nm)/ZnMgO (40 nm)/Al (100 nm), and inverted QLEDs with a structure of glass/ITO/ZnMgO (45 nm)/QDs (~15 nm)/CBP (40 nm)/MoO₃ (8 nm)/Al (100 nm) were fabricated. ITO/Al, PEDOT:PSS/MoO₃, TFB/PVK/CBP, QDs, and ZnMgO nanoparticles work as electrode, hole injection layer (HIL), hole transport layer (HTL), light emission layer (EML), and electron transport layer (ETL), respectively. The hole-only devices with a structure of glass/ITO/PEDOT:PSS (45 nm)/TFB (40 nm)/QDs (~15 nm)/Al (100 nm) were fabricated to investigate the hole injection under varied temperatures.

For the regular red QLEDs, the cleaned ITO glass substrates were treated with O₂ plasma for 6 min firstly. Next, the HILs were formed by spin-casting

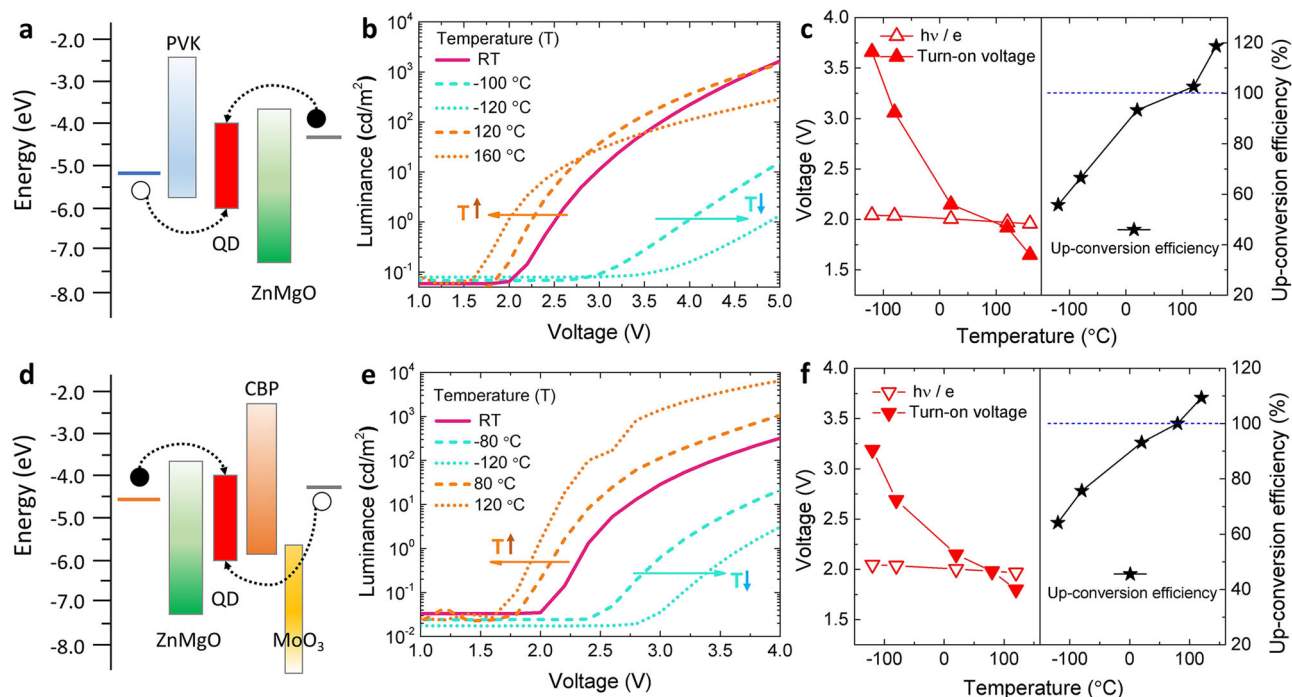


Fig. 4 The up-conversion EL in different structured QLEDs. The energy levels diagrams of **a** regular red-QLEDs with PVK HTL and **d** inverted red-QLEDs with CBP HTL. (black/white circle represents electron/hole). The L-V characteristics of **b** PVK based- and **e** CBP based-QLEDs under different temperatures: the V_T is remarkably reduced as the temperature is increased. Turn-on voltage V_T (solid triangle), photon voltage V_{ph} (open triangle) and the up-conversion efficiencies (star) of **c** PVK based- and **f** CBP based-QLEDs at different temperatures: the up-conversion efficiency is gradually increased as the temperature is increased. When the temperature is higher than 100 °C, the up-conversion efficiency of both QLEDs can exceed 100%.

PEDOT:PSS solution at 3000 rpm and baked at 130 °C for 20 min in the atmosphere. Then, the PEDOT:PSS-coated samples were transferred into a nitrogen-filled glove box to prepare the subsequent functional layers. The TFB (8 mg mL⁻¹ in chlorobenzene) HTLs were spin-coated on the top of PEDOT:PSS at 3000 rpm for 45 s and baked at 130 °C for 20 min. Subsequently, the EMLs were deposited by spin-casting the red QDs solution (15 mg mL⁻¹ in octane) at 3000 rpm and baked at 100 °C for 5 min. Afterward, ZnMgO ETLs (nanoparticles, 20 mg mL⁻¹ in ethanol) were spin-coated on QDs films at 2500 rpm and baked at 100 °C for 10 min. Finally, the coated samples were transferred to a high-vacuum evaporation chamber to deposit a 100 nm Al cathode with an evaporation rate of 5 Å s⁻¹ at a base pressure of 4×10^{-4} Pa. For the PVK HTLs, a 10 mg mL⁻¹ PVK solution in chlorobenzene was used. The regular green and blue QLEDs were fabricated by the same procedure by using a 10 mg mL⁻¹ green QDs solution (in octane), and a 10 mg mL⁻¹ blue QDs solution (in octane), respectively. For inverted red QLEDs, ZnMgO ETLs and QDs EMLs were directly deposited on ITO glass. Then, the samples were transferred to a high-vacuum evaporation chamber. At a base pressure of 4×10^{-4} Pa, CBP HTLs and MoO₃ HILs were deposited layer by layer with rates of 1.5 and 0.2 Å s⁻¹, respectively. Al anodes were deposited by the same process as conventional ones. In the end, the QLEDs were encapsulated with UV-resin and cover glass.

Characterizations. The thicknesses of the functional layers were measured using a Bruker DektakXT stylus profiler. The evaporation rates and the thicknesses of CBP, MoO₃, and Al electrode, were in situ monitored by a quartz crystal microbalance. EL spectra of QLEDs were measured by a fiber-optic spectrometer (USB 2000, Ocean Optics) in the normal direction, and the J-V-L characteristics of QLEDs were assessed by using a dual-channel Keithley 2614B programmable source meter with a PIN-25D calibrated silicon photodiode (PD) under ambient conditions. The C-V test was conducted by using an HP4284A LCR analyzer, and the frequency and amplitude of the AC signal are 1000 Hz and 0.05 V, respectively. The transient EL measurement was accomplished by using a signal generator (JunCe Instruments, JDS6600) to generate a square-wave signal (100k Hz), a PD (THORLABS, APD120A2/M) to receive lights generated by QLEDs, and a dual-channel oscilloscope (Tektronix, TBS1102) to receive the square-wave signal and the light-emitting response signal of the device.

To carry out the temperature-dependent experiments, a custom designed temperature-controllable probe station was used. Liquid nitrogen is used to control the temperature with a minimum accuracy of 0.1 °C. Temperature-dependent EL spectra/J-V-L characteristics/transient EL/C-V were all implemented using this probe station.

Reporting summary. Further information on research design is available in the Nature Research Reporting Summary linked to this article.

Data availability

The data that support the findings of this study are available from the corresponding author upon reasonable request.

Received: 25 August 2021; Accepted: 6 January 2022;

Published online: 18 January 2022

References

- Qian, L., Zheng, Y., Xue, J. G. & Holloway, P. H. Stable and efficient quantum-dot light-emitting diodes based on solution-processed multilayer structures. *Nat. Photonics* **5**, 543–548 (2011).
- Mashford, B. S. et al. High-efficiency quantum-dot light-emitting devices with enhanced charge injection. *Nat. Photonics* **7**, 407–412 (2013).
- Dai, X. L. et al. Solution-processed, high-performance light-emitting diodes based on quantum dots. *Nature* **515**, 96–99 (2014).
- Yang, Y. X. et al. High-efficiency light-emitting devices based on quantum dots with tailored nanostructures. *Nat. Photonics* **9**, 259–266 (2015).
- Shen, H. B. et al. Visible quantum dot light-emitting diodes with simultaneous high brightness and efficiency. *Nat. Photonics* **13**, 192–197 (2019).
- Pu, C. D. et al. Electrochemically-stable ligands bridge the photoluminescence-electroluminescence gap of quantum dots. *Nat. Commun.* **11**, 937 (2020).
- Won, Y. H. et al. Highly efficient and stable InP/ZnSe/ZnS quantum dot light-emitting diodes. *Nature* **575**, 634–638 (2019).
- Kim, T. et al. Efficient and stable blue quantum dot light-emitting diode. *Nature* **586**, 385–389 (2020).
- Zhang, H., Su, Q. & Chen, S. M. Quantum-dot and organic hybrid tandem light-emitting diodes with multi-functionality of full-color-tunability and white-light-emission. *Nat. Commun.* **11**, 2826 (2020).
- Zhang, H., Chen, S. M. & Sun, X. W. Efficient red/green/blue tandem quantum-dot light-emitting diodes with external quantum efficiency exceeding 21%. *ACS Nano* **12**, 697–704 (2018).

11. Su, Q., Sun, Y. Z., Zhang, H. & Chen, S. M. Origin of positive aging in quantum-dot light-emitting diodes. *Adv. Sci.* **5**, 201800549 (2018).
12. Yeh, H. J. J. & Smith, J. S. Fluidic self-assembly for the integration of GaAs light-emitting-diodes on Si substrates. *IEEE Photonics Tech. Lett* **6**, 706–708 (1994).
13. Krames, M. R. et al. High-brightness AlGaInN light-emitting diodes. *Proceedings of SPIE* **3938**, 2–12 (2000).
14. Schubert, E. F. *Light-Emitting Diodes* (Cambridge University Press, Cambridge, 2006).
15. Pandey, A. K. & Nunzi, J. M. Rubrene/fullerene heterostructures with a half-gap electroluminescence threshold and large photovoltage. *Adv. Mater.* **19**, 3613–3617 (2007).
16. Xiang, C. Y., Peng, C., Chen, Y. & So, F. Origin of sub-bandgap electroluminescence in organic light-emitting diodes. *Small* **11**, 5439–5443 (2015).
17. Engmann, S. et al. Higher order effects in organic LEDs with sub-bandgap turn-on. *Nat. Commun.* **10**, 227 (2019).
18. Qian, L. et al. Electroluminescence from light-emitting polymer/ZnO nanoparticle heterojunctions at sub-bandgap voltages. *Nano Today* **5**, 384–389 (2010).
19. Cao, W. R. et al. Highly stable QLEDs with improved hole injection via quantum dot structure tailoring. *Nat. Commun.* **9**, 2608 (2018).
20. Ji, W. Y. et al. The work mechanism and sub-bandgap-voltage electroluminescence in inverted quantum dot light-emitting diodes. *Sci. Rep.* **4**, 6974 (2014).
21. Song, J. J. et al. Over 30% External quantum efficiency light-emitting diodes by engineering quantum dot-assisted energy level match for hole transport layer. *Adv. Funct. Mater.* **29**, 1808377 (2019).
22. Luo, H. X. et al. Origin of subthreshold turn-on in quantum-dot light-emitting diodes. *ACS Nano* **13**, 8229–8236 (2019).
23. Deng, Y. et al. Deciphering exciton-generation processes in quantum-dot electroluminescence. *Nat. Commun.* **11**, 2309 (2020).
24. Sun, Y. Z. et al. Investigation on thermally induced efficiency roll-off: toward efficient and ultrabright quantum-dot light-emitting diodes. *ACS Nano* **13**, 11433–11442 (2019).
25. Liu, E. K., Zhu, B. S., & Luo, J. S. *The Physics of Semiconductors* (Publishing House of Electronics industry, Beijing, 2008).
26. Shavit, A., & Gutfinger, C. *Thermodynamics, From Concepts to Applications* (Chemical Rubber Company Press, Boca Raton, 2008).
27. Altazin, S. et al. Physics of the frequency response of rectifying organic Schottky diodes. *J. Appl. Phys.* **115**, 064509 (2014).
28. Coropceanu, V. et al. Charge transport in organic semiconductors. *Chem. Rev.* **107**, 926–952 (2007).

Acknowledgements

This work was supported by the National Natural Science Foundation of China (62174075), Shenzhen Science and Technology Program (JCYJ20210324105400002) and the Guangdong University Research Program (2020ZDZX3062).

Author contributions

S.C. conceived the idea, supervised the work and wrote the manuscript. Q.S. conducted the experiments, collected the data and drew the figures. All authors discussed the results and reviewed the manuscript.

Competing interests

The authors declare no competing interests.

Additional information

Supplementary information The online version contains supplementary material available at <https://doi.org/10.1038/s41467-022-28037-w>.

Correspondence and requests for materials should be addressed to Shuming Chen.

Peer review information *Nature Communications* thanks Jialong Zhao and the other, anonymous, reviewer(s) for their contribution to the peer review of this work.

Reprints and permission information is available at <http://www.nature.com/reprints>

Publisher's note Springer Nature remains neutral with regard to jurisdictional claims in published maps and institutional affiliations.



Open Access This article is licensed under a Creative Commons Attribution 4.0 International License, which permits use, sharing, adaptation, distribution and reproduction in any medium or format, as long as you give appropriate credit to the original author(s) and the source, provide a link to the Creative Commons license, and indicate if changes were made. The images or other third party material in this article are included in the article's Creative Commons license, unless indicated otherwise in a credit line to the material. If material is not included in the article's Creative Commons license and your intended use is not permitted by statutory regulation or exceeds the permitted use, you will need to obtain permission directly from the copyright holder. To view a copy of this license, visit <http://creativecommons.org/licenses/by/4.0/>.

© The Author(s) 2022